



Hydrodeoxygenation of Lignin-Derived Aromatic Oxygenates Over Pd-Fe Bimetallic Catalyst: A Mechanistic Study of Direct C–O Bond Cleavage and Direct Ring Hydrogenation

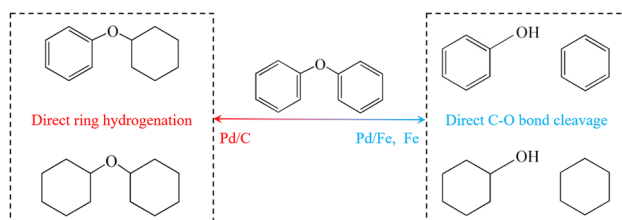
Jianghao Zhang¹ · Berlin Sudduth¹ · Junming Sun¹ · Yong Wang^{1,2}

Received: 8 June 2020 / Accepted: 4 August 2020
© Springer Science+Business Media, LLC, part of Springer Nature 2020

Abstract

Hydrodeoxygenation of lignin-derived phenols could be achieved generally with three reaction pathways: tautomerization, direct ring hydrogenation and direct C–O bond cleavage. The former pathway has been extensively studied over Pd/Fe catalyst in liquid-phase reaction, however, the contribution of the latter two is yet subject to further investigations. In this report, a comparative study of direct C–O bond cleavage and direct ring hydrogenation reaction pathways is presented on Pd/Fe, Fe and Pd/C catalysts using diphenyl ether as modelling compound. Despite its much higher activation energy than direct ring hydrogenation, direct C–O bond cleavage is dominant over Pd/Fe with much higher rates than the monometallic analogues due to the synergic catalysis of Pd–Fe. Based on this study and our previous results, the detailed reaction network for HDO of diphenyl ether is proposed.

Graphic Abstract



Keywords C–O bond cleavage · Direct ring hydrogenation · Pd–Fe catalyst · Mechanistic study · Aromatic oxygenate

Electronic supplementary material The online version of this article (<https://doi.org/10.1007/s10562-020-03352-3>) contains supplementary material, which is available to authorized users.

✉ Junming Sun
Junming.sun@wsu.edu

✉ Yong Wang
yong.wang@pnnl.gov

¹ The Gene & Linda Voiland, School of Chemical Engineering and Bioengineering, Washington State University, Pullman, WA 99164, USA

² Institute for Integrated Catalysis, Pacific Northwest National Laboratory, Richland, WA 99352, USA

1 Introduction

Hydrotreating is one of the key process in oil refining to remove heteroatoms such as sulfur, nitrogen, and oxygen [1, 2]. Similar to hydrodesulfurization and hydrodenitrogenation, which have been comprehensively studied in petroleum industry due to the consideration of environment and engine protection [3], hydrodeoxygenation (HDO) is an important research topic since the large oxygen content in bio-oil needs to be reduced to increase its energy density, stability and volatility [4].

The HDO of lignin-derived phenols is highly challenging in bio-oil upgrading and generally proceeds through three reaction pathways: tautomerization, direct ring hydrogenation and direct C–O bond cleavage [5–7]. The

tautomerization pathway involves a fast and reversible isomerization of phenols to form unstable ketone intermediates over the surface of the catalyst [8]. Accordingly, the recalcitrant $C_{\text{aromatic}}\text{-O}$ is transformed to a weaker $\text{C}=\text{O}$ bond, and the oxygen can be readily removed with a lower reaction barrier. Although this pathway is able to produce arenes, as reported in vapor-phase reactions at low pressures [8, 9], we have proven that tautomerization is the main contributor to ring saturation in liquid phase during the HDO of phenol over Pd/Fe catalysts [7]. The direct ring hydrogenation pathway usually happens over noble metal catalysts [10] that are widely utilized in HDO reactions due to their negligible barriers for H_2 dissociation. Direct ring hydrogenation commonly causes ring saturation [11, 12] because adding the first hydrogen atom to the phenyl ring has the highest barrier during aromatic ring saturation [5, 13] and once the aromaticity is broken, the remaining $\text{C}=\text{C}$ bonds can be readily saturated, especially under high H_2 pressures where the saturation is thermodynamically favored. Direct C-O bond cleavage of phenolics utilizes hydrogen most efficiently to achieve the deoxygenation though it needs to overcome a high reaction barrier [14]. However, this barrier could be lowered over oxophilic metals where the activation of $\text{C}_{\text{aromatic}}\text{-O}$ bond can be significantly facilitated by elongating the bond length [15]. After cleaving the C-O bond, the catalytic cycle is completed by hydrogenation of the phenyl and hydroxyl species to form benzene and water.

Bimetallic catalysis employing an oxophilic metal with a metal activating H_2 has been investigated and proposed as an efficient approach to HDO [9, 16–20]. Recently, vapor-phase HDO of guaiacol was studied over carbon-supported Pd–Fe catalysts [21] which displayed enhanced activity and arene selectivity without ring saturation. The synergic effect between Pd and Fe was further demonstrated using Pd-promoted Fe nanoparticles (Pd/Fe) for vapor-phase HDO of *m*-cresol, i.e. Pd assists H_2 dissociation and facilitates stabilization of the metallic Fe surface which can selectively cleavage the C-O bond [22]. The following kinetic study supports the direct C-O bond cleavage mechanism [23]. The Pd–Fe bimetallic catalysts have also been applied in the conversion of aryl ethers and shown high yield to the aromatics in both hydrogenolysis [24] and transfer hydrogenolysis [25]. However, when this Pd/Fe catalyst was applied in liquid-phase HDO, which can minimize the energy consumption, ring-saturated products dominated [7]. We systematically studied the mechanism and demonstrated that tautomerization is responsible for ring saturation during liquid-phase HDO of phenol [7].

The role of tautomerization has been well understood over Pd/Fe [7], whereas the contributions of the other two pathways over these catalysts remains unclear. Herein, we present a mechanistic study using a model reactant, diphenyl ether (DPE), which structurally inhibits tautomerization and

allows us to understand the remaining pathways, i.e. direct C-O bond cleavage and direct ring hydrogenation.

2 Experimental

2.1 Catalysts Preparation

2.1.1 Preparation of Fe_2O_3

Fe_2O_3 was synthesized by precipitation method following the previous work [22, 26]. In a typical synthesis, $(\text{NH}_4)_2\text{CO}_3$ (Sigma-Aldrich, 99.999%, 1.5M) solution was added dropwise to the solution of $\text{Fe}(\text{NO}_3)_3$ (Sigma-Aldrich, >99.99%, 3M). The dark crimson precipitate was then washed and filtrated with Milli-Q water until the pH reached 8. The obtained sample was dried at 80 °C overnight and crushed to a fine powder (sieving to <100 mesh), followed by calcination at 400 °C for 5 h.

2.1.2 Preparation of Supported 1 wt.% Pd Catalysts

Incipient wetness impregnation method was employed to prepare 1 wt.% Pd/ Fe_2O_3 . 10 wt.% $\text{Pd}(\text{NH}_3)_4(\text{NO}_3)_2$ solution (Sigma-Aldrich, 99.99%, metal basis) was diluted with Milli-Q water. This solution was then mixed with the Fe_2O_3 powder by stirring. Afterwards, the sample was dried at 80 °C overnight in air before calcination at 350 °C for 2h in flowing N_2 (50 mL/min). Monometallic Pd, 1 wt.% Pd/C was prepared following the same procedure using active carbon (TA70 PICATAL) as support.

2.2 Characterization

Transmission electron microscopy (TEM) analysis of the catalysts was carried out using an FEI Technai G2 20 Twin operated at 200 kV and equipped with a 4k Eagle CCD camera. Before the measurement, the samples were ground in a mortar for 5 min and suspended into ethanol with a sonicator, then a drop of the nanoparticle suspension was dispensed onto a 3-mm carbon-coated copper grid. Excess ethanol was removed by an absorbent paper, and the sample was dried at room temperature for 6 h.

Temperature-programmed Reduction with H_2 (H_2 -TPR) was carried out on Chemisorption Analyzer (Micromeritics AutoChem 2920) equipped with a quadrupole mass spectrometer (Omnistar gas analyzer GSD 301). Approximately 50 mg of catalyst was loaded into a quartz tube and purged with UHP Argon at a rate of 50 mL/min for 10 min. The temperature was increased to 300 °C and held for 1 h and then ramped to ambient. After this pretreatment, the flowing gas was switched to UHP H_2 at a rate of 50 mL/min and the temperature was ramped to 500 °C at 2 °C/min.

X-Ray powder diffraction (XRD) was performed on a Rigaku Miniflex II X-Ray diffractometer with $\text{Cu}_{\text{K}\alpha}$ radiation ($\lambda = 1.54178 \text{ \AA}$) operating at 40 kV and 50 mA. The scan was conducted at the rate of $1^\circ/\text{min}$ with a step-size of 0.01° from 20 to 70° .

2.3 Activity Test

Prior to the activity test, all the samples (i.e. Fe_2O_3 , Pd/C and Pd/ Fe_2O_3) were reduced ex-situ with 40 ml/min 50% H_2/N_2 at 350°C for 2 h followed by passivation with 40 ml/min 0.2% O_2/N_2 at room temperature for 1 h. Then each passivated catalyst was transferred into a glass liner in the stainless steel Parr reactor (Series 4560, 300 mL) for HDO of the DPE. After purging the reactor with 4MPa H_2 three times, the temperature was ramped to 300°C ($15^\circ\text{C}/\text{min}$) and held for another 30 min in H_2 (3 MPa) for in situ reduction. Afterwards, the reactor was cooled down to ambient temperature and the pressure was released. 6.35 mmol of DPE in 50 mL of hexadecane was then injected via syringe into the reactor. The reactor was then pressurized with H_2 and heated up to the target temperature under a stirring rate of 800 rpm for the reaction. The products were sampled periodically for analysis at the reaction temperature. Given the variable composition with temperature in the liquid phase, a linear correction assuming a constant coefficient in Henry's law was made in the concentration range studied.

Product analyses was conducted with a gas chromatograph (GC, Agilent 7890A) equipped with DB-FFAP column (30m, 0.32mm, 0.25 μm) and flame ionization detector (FID), as well as GC-MS (Shimadzu, GCMS-QP2020) equipped with a HP-5 column (30m, 0.32mm, 0.25 μm) connected to an FID. The conversion, selectivity and yield were calculated as follows: conversion [%] = (moles of carbon in the converted substrate/moles of carbon in the substrate fed) \times 100; selectivity [%] = (moles of carbon in the specific product/moles of carbon in all product) \times 100; yield [%] = (moles of carbon in the specific product/moles of carbon in the substrate fed) \times 100. The carbon balance was above 92%. The difference of conversion between 1h and the first data point was used to calculate the specific reaction rate.

3 Results and Discussions

3.1 Characterization of the Catalysts

Figure 1a, b and c display the TEM images of fresh, reduced and spent samples. The fresh sample (1 wt.% Pd/ Fe_2O_3) has a uniform size around 20 nm, being consistent with our previous study [22]. After a reduction at 350°C with 50% H_2/N_2 for 2 h, the particles of reduced Pd/Fe grow larger and are similar in size compared to the spent Pd/Fe, indicating

that the reduced catalyst is stable under reaction conditions. The reducibility was investigated with H_2 -TPR as shown in Fig. 1d. The TPR profile shows the typical two-step reactions at 166 and 339°C that are attributed to reduction of Fe_2O_3 to Fe_3O_4 and Fe_3O_4 to Fe [27]. Note that the sample was pretreated at 350°C and exposed in H_2 at 300°C during HDO, therefore the surface of catalyst should be metallic Fe modified with Pd. Fresh Pd/ Fe_2O_3 , reduced and spent Pd/Fe were characterized with XRD as shown in Fig. 1e. The pattern for the fresh samples shows its crystal structure type is hematite (JCPDS: 33-0664). After reduction and HDO reaction, the peaks for oxide disappears while the new peaks corresponding to metallic Fe (JCPDS: 06-0696) dominate. Though there is remaining oxide in the catalyst as suggested by XRD, given the sample was pretreated at 350°C and exposed in H_2 at 300°C during HDO, the surface should be metallic Fe modified with Pd. This is supported by in-situ Raman [7] and X-Ray photoelectron spectroscopy [22] in our previous study.

3.2 The Reaction Pathways

The reaction pathway was first studied over a Pd/Fe bimetallic catalyst at 300°C and 4 MPa H_2 . Fig. 2a shows the yield of each product as a function of reaction time. With increasing time-on-stream, benzene reaches a vertex and then gradually decreases likely due to slow hydrogenation over the Pd/Fe surface. The amount of cyclohexane continuously increases as a result of the slow hydrogenation of benzene and the conversion of phenol (the primary product from C–O bond cleavage of DPE) by tautomerization pathway [7]. The product selectivity versus DPE conversion is replotted and shown in Fig. 2b and c. The monomers (cyclohexane and benzene) which are derived from direct C–O bond cleavage are the major products during the entire reaction. By extrapolating the selectivity curve to 0% conversion using SPSS 22.0 software [28], the contribution of each primary reaction pathway in the reaction can be determined [29]. The direct C–O bond cleavage dominates with 94% selectivity versus 6% for direct ring hydrogenation. The reaction pathways over monometallic catalysts were also studied to gain insight into synergistic effects and how different metals influence the reacting mechanism. Over monometallic Pd (i.e., 1 wt.%Pd/C, detailed structures have been presented in previous work [22]), a comparably high activity was observed but it is mainly through direct aromatic ring hydrogenation as evidenced by the dominant formation of cyclohexyl phenyl ether (CPE) and dicyclohexyl ether (DCE), especially at low DPE conversion. As DPE conversion increases, the selectivity to cyclohexane increases at the expenses of CPE and DCE, suggesting the further hydrogenolysis of the dimers to cyclohexane. This result also suggests that the mechanism of cyclohexane formation on Pd is

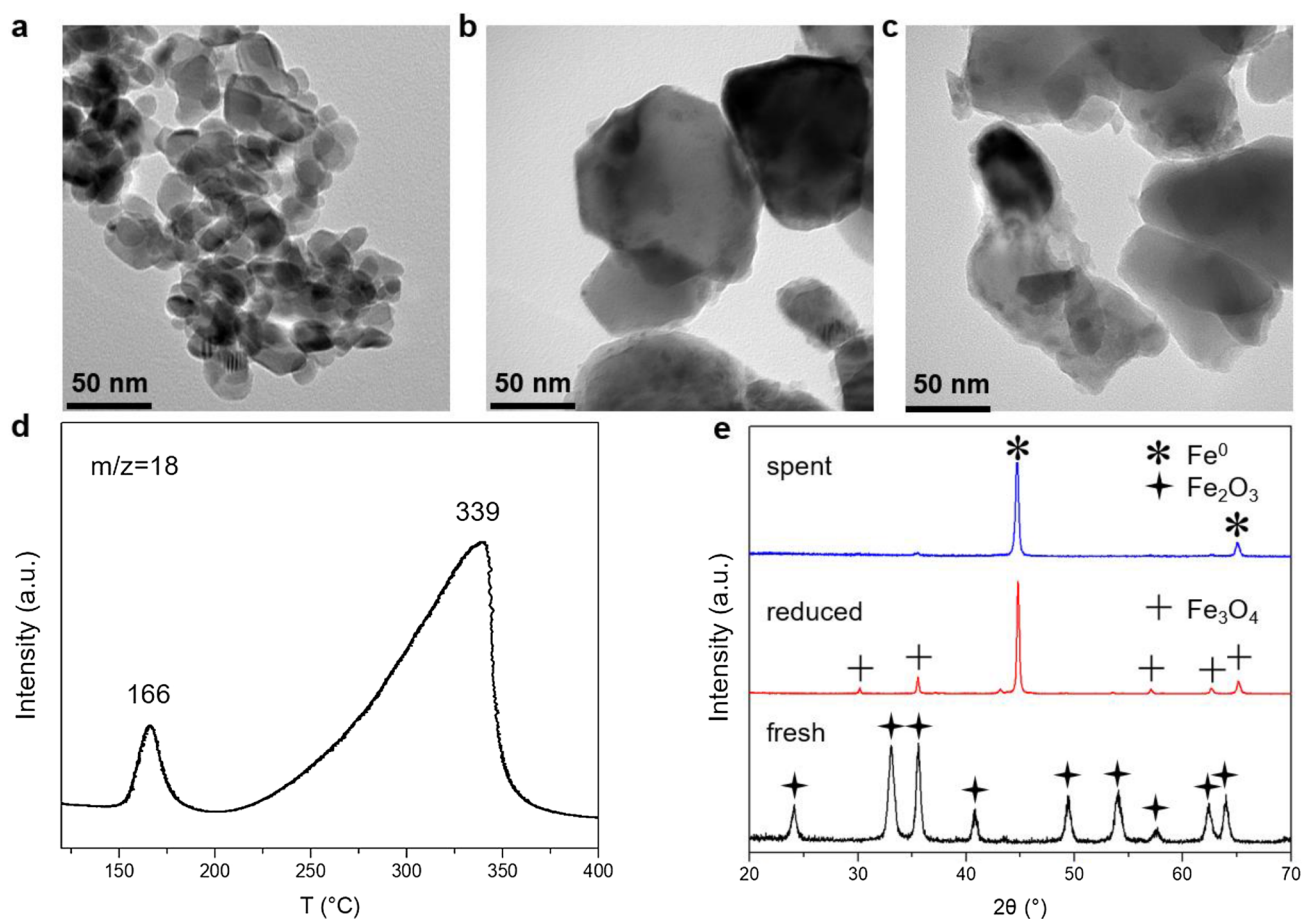


Fig. 1 Representative **a–c** TEM images of fresh 1 wt.% Pd/ Fe₂O₃, reduced Pd/Fe and spent Pd/Fe samples; **d** H₂-TPR profile of 1 wt.% Pd/Fe₂O₃; **e** XRD patterns of 1 wt.% Pd/ Fe₂O₃, reduced and spent

Pd/Fe catalysts (the patterns are scaled to produce an approximate match in intensity)

different from that on Pd/Fe and Fe in liquid-phase reactions. Using the same extrapolation method, the selectivities at 0% conversion for direct C–O bond cleavage and direct ring saturation were determined to be 22% and 78%, respectively. Over monometallic Fe catalyst (the structure has been studied in previous work [22]), despite its low activity, no direct aromatic ring hydrogenation and only direct C–O cleavage was observed (Fig. 2g–i). Table 1 summarizes the reaction rates for direct C–O bond cleavage and direct ring hydrogenation over these three catalysts. Pd/C displayed a C–O cleavage (22% selectivity) rate of 0.29 mmol/h at 300 °C, while Fe only showed a rate of 0.27 mmol/h with 100% selectivity. In contrast, Pd/Fe catalyst not only maintained high selectivity (94%), but also exhibited the highest rate for direct C–O cleavage (2.64 mmol/h). The above results indicate that the dominant reaction pathway differs over these three catalysts. Pd primarily hydrogenates the aromatic ring with high reaction rates while Fe primarily cleaves the C–O bond with lower rates. The synergy between Pd and Fe significantly enhanced activity while maintaining the

high C–O bond cleavage selectivity observed on Fe. On the other hand, Fe also modified the Pd [30], leading to inhibited activity for aromatic ring saturation (0.17 mmol/h for Pd/Fe and 1.02 mmol/h for Pd/C) though the two catalysts expose same amount of Pd. This synergy between Pd and Fe has also been found in the vapor-phase HDO of phenols (i.e., guaiacol [21], cresol [22]).

3.3 Activation Energies for the Two Pathways

To understand the energy profile of the two pathways, Arrhenius plot for HDO of DPE was derived as shown in Fig. 3. The two parallel reactions displayed distinct apparent activation energies (E_a): 46 kJ/mol for direct hydrogenation and 86 kJ/mol for direct C–O cleavage of DPE. Wang et al. [31] studied cresol HDO over Mo-based catalysts and measured the E_a for direct deoxygenation through C–O bond cleavage as 125 kJ/mol and hydrogenation followed by deoxygenation as 89 kJ/mol. These results display the same trend that the E_a for direct C–O bond cleavage is much higher than that

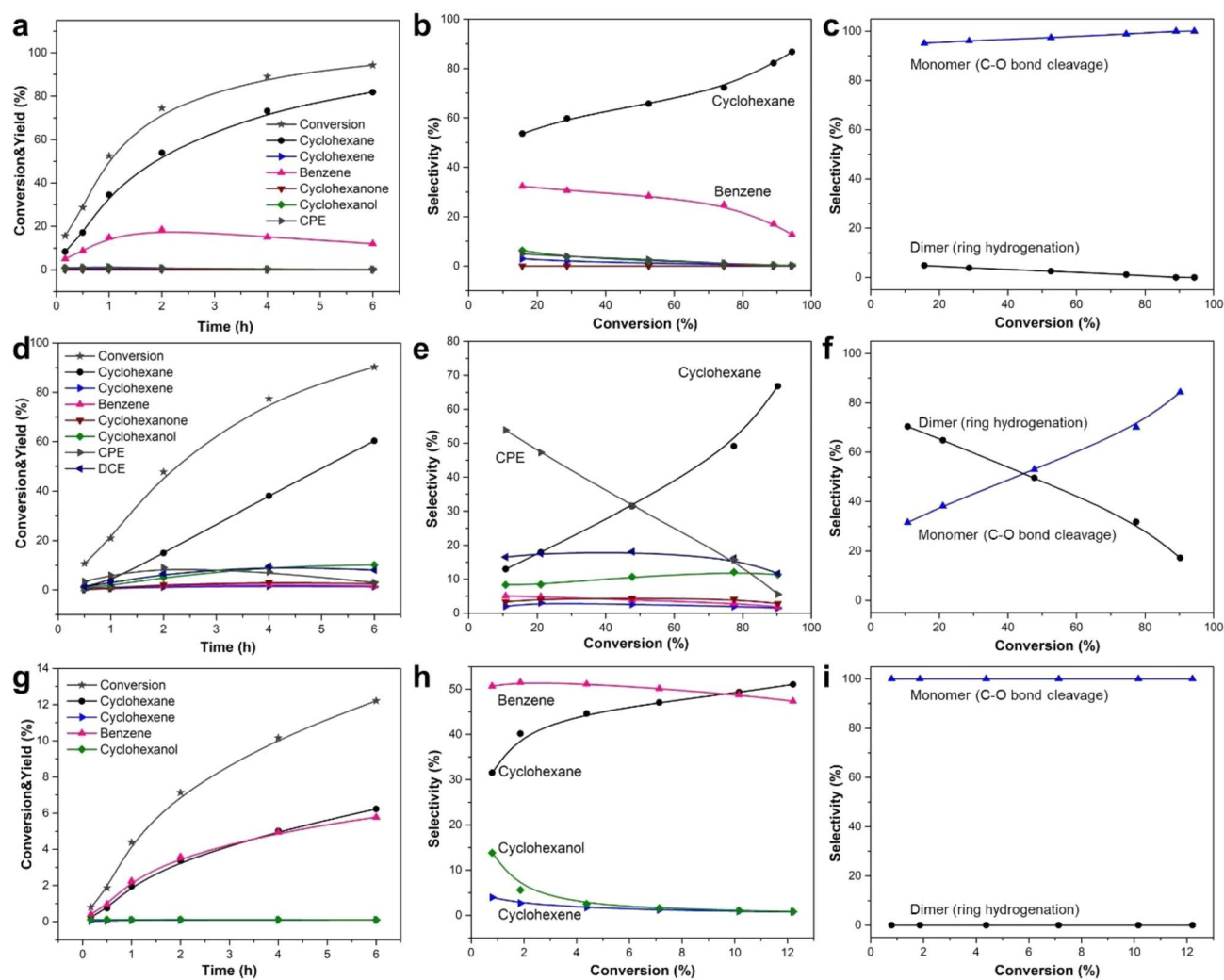


Fig. 2 The DPE conversion over Pd/Fe (a–c, data taken from ref[7]), Pd/C (d–f) and Fe (g–i) catalysts. **a, d, g**, Conversion and yield of each products as a function of reacting time; **b, e, h**, Product distribution as a function of DPE conversion; **c, f, i**, Selectivity of monomers (from direct C–O bond cleavage) and ring-saturated dimers (from direct ring hydrogenation) as a function of conversion. The amount

of 1%Pd/C were determined to expose same amount of Pd as Pd/Fe according to the CO-TPD results (Fig. S1). Catalysts amounts: 150 mg for Pd/Fe, 20 mg for Pd/C and 150 mg for Fe. Reaction condition: 300 °C, 6.35 mmol diphenyl ether (1 mL), 50 mL hexadecane, 6MPa H₂

for ring hydrogenation. The E_a for DPE HDO is lower than cresol, likely due to the much lower C–O bond dissociation energy of DPE [32]. Note that although the direct hydrogenation has a much smaller activation barrier, its reaction rate is still lower than direct C–O cleavage in the tested range of temperature. This suggests that the pre-exponential factor in the Arrhenius rate law and the amounts of active sites for direct ring-hydrogenation should be much smaller than that of C–O cleavage.

3.4 Reaction Mechanism

Based on the above results and our previous study [7], the pathway of catalytic conversion of DPE is proposed

as shown in Scheme 1. Overall, there are two parallel primary routes under the studied reaction conditions: direct C–O bond cleavage, which mainly exists over Pd/Fe and Fe catalysts (Fig. 2c and i), and direct ring hydrogenation, which mainly exists over Pd/C catalyst (Fig. 2f). In the direct C–O bond cleavage route, the primary product, phenol, is converted via tautomerization and hydrogenation to form cyclohexanone and cyclohexadienol which are subsequently converted to cyclohexanol, followed by C–O bond cleavage to form cyclohexane [7]. However, over Pd/C catalyst, DPE is primarily hydrogenated to form CPE. The formed CPE is then converted via C–O bond cleavage, as evidenced in Fig. 2d–e and Fig. S2. Given

Table 1 Catalytic performances of the Pd/C, Fe and Pd/Fe catalysts for the HDO of DPE. Reaction condition: 300 °C, 6.35 mmol diphenyl ether (1 mL), 50 mL hexadecane, 6 MPa H₂

Catalyst	Specific rate of C-O cleavage (mmol/h)	Specific rate of ring hydrogenation (mmol/h)	Selectivity at 0% conversion ^a	
			C-O cleavage (%)	Hydrogenation (%)
Pd/Fe	2.64	0.17	94	6
Fe	0.27	0	100	0
Pd/C ^b	0.29	1.02	22	78

^aSelectivity was derived by extrapolating the curve in Fig. 2c, f, i to conversion = 0.

^bThe amount of catalysts was determined to expose same amount of Pd according to the CO-TPD results (Fig. S1). Catalysts amounts: 150 mg for Pd/Fe, 20 mg for Pd/C and 150 mg for Fe.

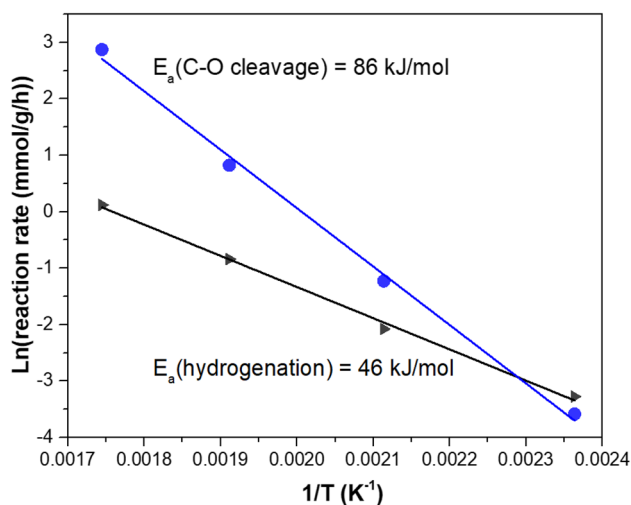


Fig. 3 Arrhenius plot for direct ring hydrogenation and C–O cleavage of diphenyl ether (data was derived at 150 °C, 200 °C, 250 °C, 300 °C). Reaction condition: 6.35 mmol diphenyl ether (1 mL), 50 mL hexadecane, 6MPa H₂

the lower bond dissociation energy of C_{aliphatic}–O comparing with that of C_{aromatic}–O in CPE [33], C_{aliphatic}–O is cleaved forming cyclohexane and phenol. The phenol is further converted to cyclohexanol by direct ring hydrogenation or tautomerization pathways, and subsequently to cyclohexane/cyclohexene. In parallel, the hydrogenation

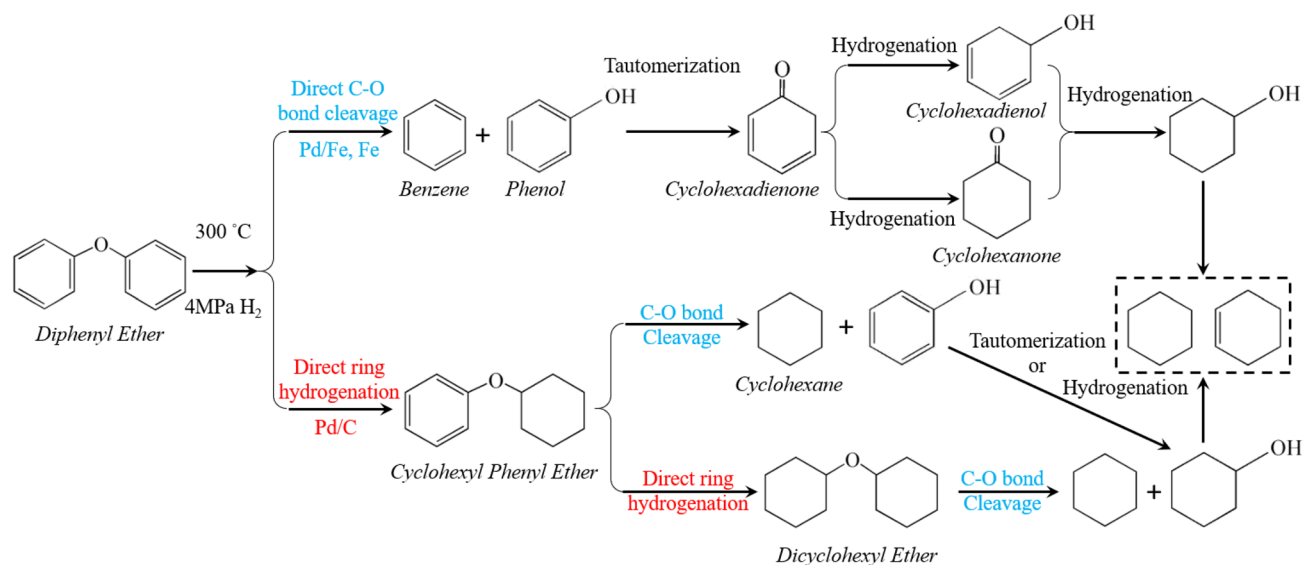
of CPE also occurs leading to the formation of DCE. Note that, due to its high bond energy, the C–O bond in DCE could hardly be cleaved on Pd at low temperature (e.g. 200 °C [34]). Herein, at 300 °C and 6MPa pressure, it is found that hydrogenolysis of DCE slowly occurs to form cyclohexanol, cyclohexene and cyclohexane, as evidenced in Fig. 2d–e and Fig. S2.

3.5 Stability of Pd/Fe

The stability of Pd/Fe catalyst was further tested using HDO of diphenyl ether at 300 °C and 6 MPa H₂, as shown in Fig. 4. After one cycle of reaction, the catalyst was washed with ethanol, followed by drying at 50 °C overnight. In four tested cycles, the conversion and deoxygenation selectivity are maintained at around 55% and 97%, respectively. The good stability of catalytic performance is in agreement with the TEM images that show no obvious change of the particle size when comparing the fresh and spent catalysts. More importantly, the high stability indicates that there is no surface reconstruction nor change in active site during the reaction. Thus, the change of product concentration during HDO in the above study is exclusively attributed to intrinsic catalytic processes over stable active sites.

4 Conclusion

A comparative study of direct C–O bond cleavage and direct ring hydrogenation reaction pathways has been conducted over Pd/Fe, Fe and Pd/C catalysts with a modelling compound: diphenyl ether (a molecule that is exclusively converted via two pathways during HDO). Although direct C–O bond cleavage has higher apparent activation energy than direct ring hydrogenation, Pd/Fe catalysts display a synergic effect resulting in enhanced reaction rate and high direct C–O cleavage selectivity. This is likely due to the surface of this catalyst is dominated with the active sites selective for direct C–O bond cleavage. A detailed reaction network is proposed where Pd/Fe and Fe mainly catalyze the direct C–O bond cleavage of DPE and the produced phenol is then converted through the tautomerization pathway; in contrast, monometallic Pd mainly catalyzes direct ring hydrogenation.



Scheme 1 Proposed reaction pathway for the HDO of DPE

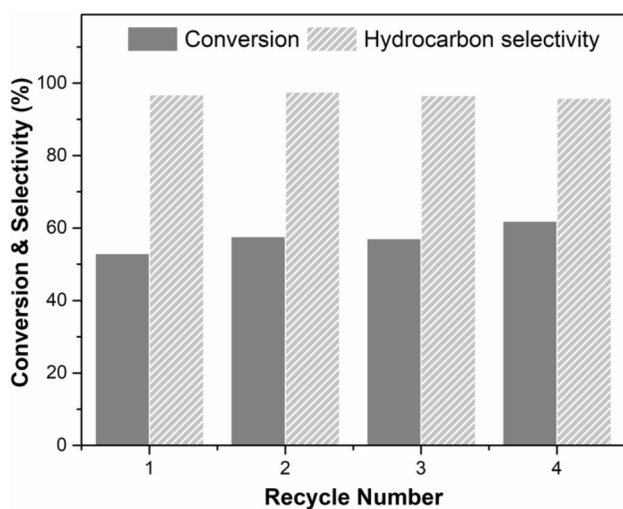


Fig. 4 Pd/Fe performance for HDO of DPE at each cycle. Reaction condition: 300 °C, 50 mg catalyst, 6.35 mmol diphenyl ether (1 mL), 50 mL hexadecane, 6MPa H₂, 4h

Acknowledgements This work was supported by the U.S. Department of Energy (DOE), Office of Science, Basic Energy Sciences (BES) and Division of Chemical Sciences, Biosciences and Geosciences (DE-AC05-RL01830, FWP-47319). The authors thank the Franceschi Microscopy and Imaging Center (FMIC) in Washington State University for the access to TEM.

Data Availability The datasets generated during and/or analysed during the current study are available from the corresponding author on reasonable request.

Compliance with Ethical Standards

Conflict of interest The authors declare that they have no conflict of interest.

Reference

- Wang H, Male J, Wang Y (2013) Recent advances in hydrotreating of pyrolysis bio-oil and its oxygen-containing model compounds. *ACS Catal* 3(5):1047–1070
- Yuan Y, Zhang J, Chen H, Hou Q, Shen J (2019) Preparation of Fe₂P/Al₂O₃ and FeP/Al₂O₃ catalysts for the hydrotreating reactions. *J Energy Chem* 29:116–121
- Clark P, Oyama S (2003) Alumina-supported molybdenum phosphide hydroprocessing catalysts. *J Catal* 218(1):78–87
- Ojagh H, Creaser D, Salam MA, Grennfelt EL, Olsson L (2019) The effect of rosin acid on hydrodeoxygenation of fatty acid. *J Energy Chem* 28:85–94
- Gu GH, Mullen CA, Boateng AA, Vlachos DG (2016) Mechanism of dehydration of phenols on noble metals via first-principles microkinetic modeling. *ACS Catal* 6(5):3047–3055
- Griffin MB, Ferguson GA, Ruddy DA, Bidy MJ, Beckham GT, Schaidle JA (2016) Role of the support and reaction conditions on the vapor-phase deoxygenation of m-cresol over Pt/C and Pt/TiO₂ catalysts. *ACS Catal* 6(4):2715–2727
- Zhang J, Sun J, Sudduth B, Pereira Hernandez X, Wang Y (2020) Liquid-phase hydrodeoxygenation of lignin-derived phenolics on Pd/Fe: a mechanistic study. *Catal Today* 339:305–311
- Nie L, Resasco DE (2014) Kinetics and mechanism of m-cresol hydrodeoxygenation on a Pt/SiO₂ catalyst. *J Catal* 317:22–29
- Nie L, de Souza PM, Noronha FB, An W, Sooknoi T, Resasco DE (2014) Selective conversion of m-cresol to toluene over bimetallic Ni–Fe catalysts. *J Mol Catal A* 388–389:47–55
- Robinson A, Ferguson GA, Gallagher JR, Cheah S, Beckham GT, Schaidle JA, Hensley JE, Medlin JW (2016) Enhanced hydrodeoxygenation of m-cresol over bimetallic Pt–Mo catalysts through

- an oxophilic metal-induced tautomerization pathway. *ACS Catal* 6(7):4356–4368
11. Nguyen T-S, Laurenti D, Afanasiev P, Konuspayeva Z, Piccolo L (2016) Titania-supported gold-based nanoparticles efficiently catalyze the hydrodeoxygenation of guaiacol. *J Catal* 344:136–140
 12. Zhao C, He J, Lemonidou AA, Li X, Lercher JA (2011) Aqueous-phase hydrodeoxygenation of bio-derived phenols to cycloalkanes. *J Catal* 280(1):8–16
 13. Yoon Y, Rousseau R, Weber RS, Mei D, Lercher JA (2014) First-principles study of phenol hydrogenation on Pt and Ni catalysts in aqueous phase. *J Am Chem Soc* 136(29):10287–10298
 14. Hus M, Bjelic A, Grilc M, Likozar B (2018) First-principles mechanistic study of ring hydrogenation and deoxygenation reactions of eugenol over Ru(0001) catalysts. *J Catal* 358:8–18
 15. Liu XY, An W, Turner CH, Resasco DE (2018) Hydrodeoxygenation of m-cresol over bimetallic NiFe alloys: kinetics and thermodynamics insight into reaction mechanism. *J Catal* 359:272–286
 16. Pino N, Sitthisa S, Tan Q, Souza T, López D, Resasco DE (2017) Structure, activity, and selectivity of bimetallic Pd-Fe/SiO₂ and Pd-Fe/ γ -Al₂O₃ catalysts for the conversion of furfural. *J Catal* 350:30–40
 17. Huang Y-B, Yan L, Chen M-Y, Guo Q-X, Fu Y (2015) Selective hydrogenolysis of phenols and phenyl ethers to arenes through direct C-O cleavage over ruthenium–tungsten bifunctional catalysts. *Green Chem* 17(5):3010–3017
 18. de Souza PM, Rabelo-Neto RC, Borges LEP, Jacobs G, Davis BH, Sooknoi T, Resasco DE, Noronha FB (2015) Role of keto intermediates in the hydrodeoxygenation of phenol over Pd on oxophilic supports. *ACS Catal* 5(2):1318–1329
 19. Wang C, Mironenko AV, Raizada A, Chen TQ, Mao XY, Padmanabhan A, Vlachos DG, Gorte RJ, Vohs JM (2018) Mechanistic study of the direct hydrodeoxygenation of m-cresol over WO_x-decorated Pt/C catalysts. *ACS Catal* 8(9):7749–7759
 20. Shao Y, Xia Q, Dong L, Liu X, Han X, Parker SF, Cheng Y, Daelen LL, Ramirez-Cuesta AJ, Yang S, Wang Y (2017) Selective production of arenes via direct lignin upgrading over a niobium-based catalyst. *Nat Commun* 8:16104
 21. Sun J, Karim AM, Zhang H, Kovarik L, Li XS, Hensley AJ, McEwen J-S, Wang Y (2013) Carbon-supported bimetallic Pd-Fe catalysts for vapor-phase hydrodeoxygenation of guaiacol. *J Catal* 306:47–57
 22. Hong Y, Zhang H, Sun J, Ayman KM, Hensley AJR, Gu M, Engelhard MH, McEwen J-S, Wang Y (2014) Synergistic catalysis between Pd and Fe in gas phase hydrodeoxygenation of m-cresol. *ACS Catal* 4(10):3335–3345
 23. Hong Y, Wang Y (2017) Elucidation of reaction mechanism for m-cresol hydrodeoxygenation over Fe based catalysts: a kinetic study. *Catal Commun* 100:43–47
 24. Kim JK, Lee JK, Kang KH, Song JC, Song IK (2015) Selective cleavage of CO bond in benzyl phenyl ether to aromatics over Pd-Fe bimetallic catalyst supported on ordered mesoporous carbon. *Appl Catal A* 498:142–149
 25. Paone E, Espro C, Pietropaolo R, Mauriello F (2016) Selective arene production from transfer hydrogenolysis of benzyl phenyl ether promoted by a co-precipitated Pd/Fe₃O₄ catalyst. *Catal Sci Technol* 6(22):7937–7941
 26. Zhang J, Sun J, Kovarik L, Engelhard MH, Du L, Sudduth B, Li H, Wang Y (2020) Surface engineering of earth-abundant Fe catalysts for selective hydrodeoxygenation of phenolics in liquid phase. *Chem Sci* 11(23):5874–5880
 27. Zieliński J, Zglinicka I, Znak L, Kaszkur Z (2010) Reduction of Fe₂O₃ with hydrogen. *Appl Catal A* 381(1–2):191–196
 28. Wang L, Chen X, Liang J, Chen Y, Pu X, Tong Z (2009) Kinetics of the catalytic isomerization and disproportionation of rosin over carbon-supported palladium. *Chem Eng J* 152(1):242–250
 29. Feitosa LF, Berhault G, Laurenti D, Davies TE, Teixeira da Silva V (2016) Synthesis and hydrodeoxygenation activity of Ni₂P/C—effect of the palladium salt on lowering the nickel phosphide synthesis temperature. *J Catal* 340:154–165
 30. Hensley AJR, Hong Y, Zhang R, Zhang H, Sun J, Wang Y, McEwen J-S (2014) Enhanced Fe₂O₃ reducibility via surface modification with Pd: characterizing the synergy within Pd/Fe catalysts for hydrodeoxygenation reactions. *ACS Catal* 4(10):3381–3392
 31. Wang H, Liu S, Smith KJ (2016) Synthesis and hydrodeoxygenation activity of carbon supported molybdenum carbide and oxycarbide catalysts. *Energy Fuel* 30(7):6039–6049
 32. Prasomsri T, Shetty M, Murugappan K, Román-Leshkov Y (2014) Insights into the catalytic activity and surface modification of MoO₃ during the hydrodeoxygenation of lignin-derived model compounds into aromatic hydrocarbons under low hydrogen pressures. *Energy Environ Sci* 7(8):2660–2669
 33. Si X-G, Zhao Y-P, Song Q-L, Cao J-P, Wang R-Y, Wei X-Y (2020) Hydrogenolysis of lignin-derived aryl ethers to monomers over a MOF-derived Ni/N-C catalyst. *React Chem Eng* 5(5):886–895
 34. Wang M, Gutierrez OY, Camaioni DM, Lercher JA (2018) Palladium-catalyzed reductive insertion of alcohols into aryl ether bonds. *Angew Chem Int Ed* 57(14):3747–3751

Publisher's Note Springer Nature remains neutral with regard to jurisdictional claims in published maps and institutional affiliations.